7-14-2023

Mesenchymal Stem Cell-Extracellular Vesicle Therapy for Stroke: Scalable Production and Imaging Biomarker Studies

Jeong Pyo Son

Eun Hee Kim

Eun Kyoung Shin

Dong Hee Kim

Ji Hee Sung

See next page for additional authors

Authors

Jeong Pyo Son, Eun Hee Kim, Eun Kyoung Shin, Dong Hee Kim, Ji Hee Sung, Mi Jeong Oh, Jae Min Cha, Michael Chopp, and Oh Young Bang

Mesenchymal Stem Cell-Extracellular Vesicle Therapy for Stroke: Scalable Production and Imaging Biomarker Studies

Jeong Pyo Son, Eun Hee Kim, Eun Kyoung Shin, Dong Hee Kim, Ji Hee Sung, Mi Jeong Oh, Jae Min Cha, Michael Chopp, Oh Young Bang

Stem Cells Translational Medicine, 2023, **12**, 459–473
https://doi.org/10.1093/stcltm/szad034
Advance access publication 13 June 2023
Original Research

Mesenchymal Stem Cell-Extracellular Vesicle Therapy for Stroke: Scalable Production and Imaging Biomarker Studies

Jeong Pyo Son[1,2,3,‡], Eun Hee Kim[2,4,‡], Eun Kyoung Shin[2,4], Dong Hee Kim[1,2], Ji Hee Sung[2,4], Mi Jeong Oh[2], Jae Min Cha[5], Michael Chopp[6], Oh Young Bang[*,1,2,4,7]

[1]Department of Health Sciences and Technology, Samsung Advanced Institute for Health Sciences and Technology (SAIHST), Sungkyunkwan University, Seoul, South Korea
[2]Stem Cell and Regenerative Medicine Institute, Samsung Medical Center, Seoul, South Korea
[3]Accelerator Radioisotope Research Section, Advanced Radiation Technology Institute (ARTI), Korea Atomic Energy Research Institute (KAERI), Jeongeup, South Korea
[4]R&D Division, S&E bio Co., Ltd., Seoul, South Korea
[5]3D Stem Cell Bioprocessing Laboratory, Department of Mechatronics, Incheon National University, Incheon, South Korea
[6]Department of Neurology, Henry Ford Health System, Detroit, MI, USA
[7]Department of Neurology, Samsung Medical Center, Sungkyunkwan University School of Medicine, South Korea

*Corresponding author: Oh Young Bang, MD, PhD, Department of Neurology, Samsung Medical Center, Sungkyunkwan University, 81 Irwon-ro, Gangnam-gu, Seoul 135-710, South Korea. Tel: +82 2 3410 3599; Fax: +82 2 3410 0052; Email: ohyoung.bang@samsung.com
‡J.P.S. and E.H.K. contributed equally.

Abstract

A major clinical hurdle to translate MSC-derived extracellular vesicles (EVs) is the lack of a method to scale-up the production of EVs with customized therapeutic properties. In this study, we tested whether EV production by a scalable 3D-bioprocessing method is feasible and improves neuroplasticity in animal models of stroke using MRI study. MSCs were cultured in a 3D-spheroid using a micro-patterned well. The EVs were isolated with filter and tangential flow filtration and characterized using electron microscopy, nanoparticle tracking analysis, and small RNA sequencing. Compared to conventional 2D culture, the production-reproduction of EVs (the number/size of particles and EV purity) obtained from 3D platform were more consistent among different lots from the same donor and among different donors. Several microRNAs with molecular functions associated with neurogenesis were upregulated in EVs obtained from 3D platform. EVs induced both neurogenesis and neuritogenesis via microRNAs (especially, miR-27a-3p and miR-132-3p)-mediated actions. EV therapy improved functional recovery on behavioral tests and reduced infarct volume on MRI in stroke models. The dose of MSC-EVs of 1/30 cell dose had similar therapeutic effects. In addition, the EV group had better anatomical and functional connectivity on diffusion tensor imaging and resting-state functional MRI in a mouse stroke model. This study shows that clinical-scale MSC-EV therapeutics are feasible, cost-effective, and improve functional recovery following experimental stroke, with a likely contribution from enhanced neurogenesis and neuroplasticity.

Key words: stroke; stem cells; extracellular vesicles; magnetic resonance imaging; neurogenesis.

Received: 13 December 2022; Accepted: 15 April 2023.

Graphical Abstract

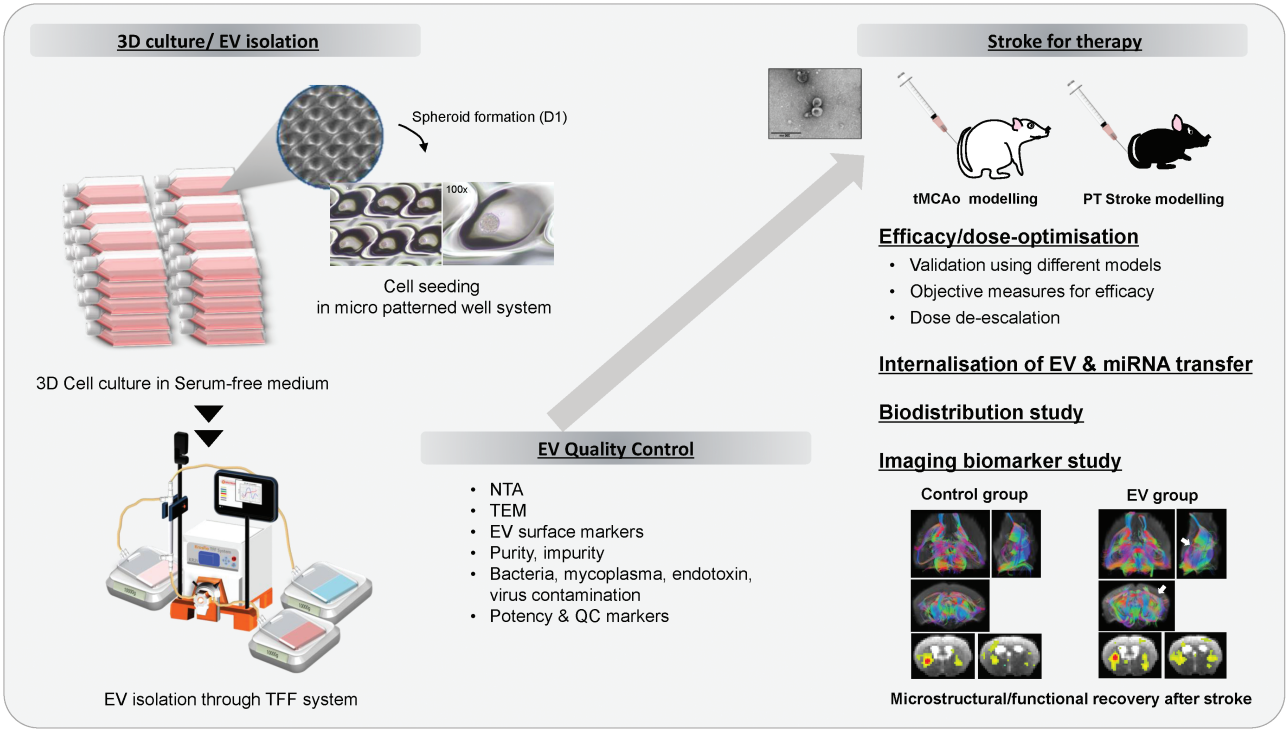

This summary shows efficient and scalable EV production method for stroke therapy using a 3D platform, which enhances neurogenesis-related microRNAs. The therapeutic benefits of EVs include improved functional recovery and brain connectivity changes, likely due to increased neuroplasticity mediated by miR-27a-3p and miR-132-3p in the EV cargo.

Significance Statement

Our scalable EV production method using a 3D platform is feasible, improves production-reproduction, and upregulates several microRNAs with molecular functions associated with neurogenesis. EVs improve functional recovery following experimental stroke, with a likely contribution from enhanced neurogenesis and neuroplasticity revealed by brain microstructural and functional connectivity changes on MRI. EV cargo, especially the miR-27a-3p and miR-132-3p, mediates these therapeutic effects.

Introduction

Stroke is the leading cause of physical disability among adults. Stem cell therapy is a potential regenerative strategy for recovery after stroke. Mesenchymal stem cells (MSCs) exert their paracrine action via secretomes or extracellular vesicles (EVs) in stroke. A cell-free treatment paradigm using stem cell-derived EVs has low toxicity and is safer than traditional cell therapy approaches by avoiding stem cell-related problems such as vascular occlusion, coagulopathy, and tumor formation.[1-4] EVs have low toxicity, high stability in the circulation, and high transport efficiency to recipient cells, with an ability to cross the blood-brain barrier, thus avoiding the first-pass effect.[5] We have shown that treatment of ischemic stroke patients with MSCs significantly increases circulating EVs, which were significantly correlated with improvement in motor function and magnetic resonance imaging (MRI) indices of plasticity.[6] The development of MSC-derived EVs into a viable "off-the-shelf" therapeutic would allow for their use during the acute phase following stroke, thus providing both neurorestorative and neuroprotective action.

Critical hurdles remain to translate MSC-EVs into a clinical therapeutic. Several good manufacturing practice (GMP) compliant and scalable MSC-EVs or MSC-secretome production have been reported.[7-9]. However, these studies used the EV preparations obtained from conventional 2D culture of MSCs. We have previously reported that MSCs 3D-cultured as size-controlled cellular aggregates on a large-scale better preserved the innate phenotype and properties of MSCs more than 2D monolayer cultures, which resulted in the significantly augmented secretion of therapeutic MSC-derived EVs and their therapeutic contents (miRNAs and cytokines) from MSCs compared to the conventional 2D culture.[10]

In the present study, we hypothesized that a 3D micro-patterned well system can be used for clinical scale EV production, and an EV therapeutic improves morphological and connectivity outcomes in animal models of stroke. To this end, we developed EV-bioprocessing platform designed using a cell non-adhesive microwell-patterned array for the scalable production of human Wharton's Jelly (WJ)-MSC-derived EVs with serum-free media and compared the production-reproduction of EVs (the number/size of particles numbers and EV purity) between EVs obtained from 3D culture system using a micro-patterned well system (3D-EV) and EVs produced from conventional 2D-cultured MSCs (natural EV).

In addition, we evaluated their effects on functional recovery and neuroplasticity after stroke using MRI measurements (including T_2-weighted MRI, diffusion tensor imaging [DTI], and resting-state functional MRI [rs-fMRI]) following intravenous injection of 3D-EVs after experimental stroke.

Materials and Methods

All the tests were carried out and documented according to validated standard operating procedures. The lists and details of experiments for clinical scale EV therapy are provided in Supplementary Table S1.

All research using human subjects was approved by the Institutional Review Board (*Samsung Medical Center Institutional Review Board*). WJ was obtained from healthy 3 volunteers. All volunteers or their named guardians provided written informed consent to participate in this study (IRB file No. 2016-07-102). Our research complied with the regulatory requirements for human cells, tissues, and cellular and tissue-based products (HCT/Ps) regulated in compliance under section CFR 1271 Title 21 "361" of PHS of the US FDA. All animal experimental procedures were approved by the Institutional Animal Care and Use Committee (*Laboratory Animal Research Center; an AAALAC International approved facility*) of Samsung Medical Center and performed in accordance with the Animal Research: Reporting of in vivo experiments (ARRIVE) guidelines.[11] All animals were kept under the conditions of a temperature of 22 ± 1 °C, a relative humidity of 50% ± 10%, a lighting time of 12 h (8 a.m. to 8 p.m.), a ventilation frequency of 10-20 times/h, and an illuminance of 150-300 Lux. All animals were observed twice daily for health monitoring and no adverse events occurred. A completed ARRIVE guidelines checklist is included in S10 ARRIVE Checklist.

Both transient and permanent animal stroke models, a rat stroke model of 90 min transient middle cerebral artery occlusion (tMCAo) and a mouse photothrombotic (PT) stroke model, were used to confirm the effects of EVs on functional recovery after stroke (Fig. 1). The rat tMCAo model of stroke was used for immunohistochemistry and dose de-escalation testing to identify the minimal effective EV dose. Serial morphological and connectivity changes were measured by MRI after treatment with a minimal effective dose of EVs vs. a control in a PT stroke mouse model.

Preparation of EVs

Umbilical Cord Wharton's Jelly-Derived Mesenchymal Stem Cells

The details of master cell banking are described in Supplementary Data.

Three-Dimensional (3D) Spheroid Culture of the WJ-MSCs

The MSCs derived from human WJ of the umbilical cord (WJ-MSC) were culture expanded at passage 5 with growth medium in a 5% CO_2 incubator at 37 °C. The WJ-MSCs were used at passage 6 to generate 3D spheroid cultures. To seed the WJ-MSCs into a micro-patterned well system (the EZSPHERE, ReproCELL Inc., Tokyo, Japan), the cells were washed with phosphate-buffered saline (PBS) and trypsinized using TrypLE Express (GIBCO). After the WJ-MSCs were centrifuged, fresh serum-free medium without heterologous protein was added and the cells were counted using a hemocytometer. After cell counting, 60 mL of cell suspension was placed in a microarray containing about 69 000 microwells each with a diameter and depth of 500 μm × 200 μm coated with MPC (2-methacryloyloxyethyl phosphorylcholine polymer) at a density of 400 cells/well. For 3D spheroid culture of WJ-MSC, serum-free medium (a-MEM) was used; and an antibiotic was not included. Three-dimensional spheroidal cell aggregates were prepared by inducing spontaneous spheroidal cell aggregate formation while maintaining a static state by dispensing as uniformly as possible and culturing in a CO_2 incubator at 37 °C for a total of 4 days.

To select optimal culture conditions for high production yield and quality, cell viability and EV yield were compared through trypan blue staining for each culture period from 1 to 7 days after 3D spheroid formation. As the culture period elapsed, EV yield showed a tendency to increase, but cell viability decreased after 5 days. Considering both viability of source cells and the yield of EV production, the culturing period was set to 4 days; cell viability, determined by trypan blue staining at the end of harvest, was greater than 83% (data not shown). After incubation, uniformity (roundness and solidity) was confirmed by quantifying the morphology and size of the spheroid, and then cells and cultured medium were recovered to confirm cell viability in the spheroid. The spheroid morphology was assessed as (a) roundness, an indicator of the circularity of the projected area of the spheroids (ranges from 0 to 1, and values closer to 1 indicate high circularly of the projected area) and (b) solidity, an indicator of the roughness of the spheroid surface and provide information on the regularity of the aggregate (a spheroid is considered regular for solidity values higher than 0.9).

Isolation of EVs

EV isolation was performed in biological safety cabinet (BSC). Culture medium was collected by gentle pipetting at the top of the wells. To remove cell debris and apoptotic bodies, 1800 mL of culture medium was centrifuged at 2500 × *g* for 10 min, followed by filtration through a 0.22-μm membrane. The filtered medium was separated using a 300-kDa MWCO mPES hollow fiber MiniKros filter module (Spectrum Laboratories, Rancho Dominguez, CA, USA) on a commercially available KrosFlo KR2I tangential flow filtration (TFF) system (Spectrum Laboratories, Rancho Dominguez) that allows for large-scale processing of samples. The EV-containing sample was recirculated into the filtration bottle. Small molecules, including free protein, were passed through the membrane pores, eluted as permeate, and collected. The collected solution was used as a secretome. EVs were maintained in circulation as retentate and concentrated in the bag. The shear rate of the feed stream was maintained between 3000 s^{-1} and 6000 s^{-1}; trans-membrane pressure was performed 7.5 psi. We conducted 5 volume exchanges of EVs with PBS and EVs were subsequently concentrated into a final volume of 300 mL of recovery solution (PBS). The recovered solution was filtered through a 0.22-μm membrane. After harvesting the conditioned media, EV isolation process was immediately started with TFF procedure.

All processes were performed according to the current guidelines on quality, non-clinical, and clinical assessment of EV therapy products by the Korean Food and Drug Administration (FDA, released Dec 2018), and using GMP-compliant methods (Supplementary Table S1). The schematics

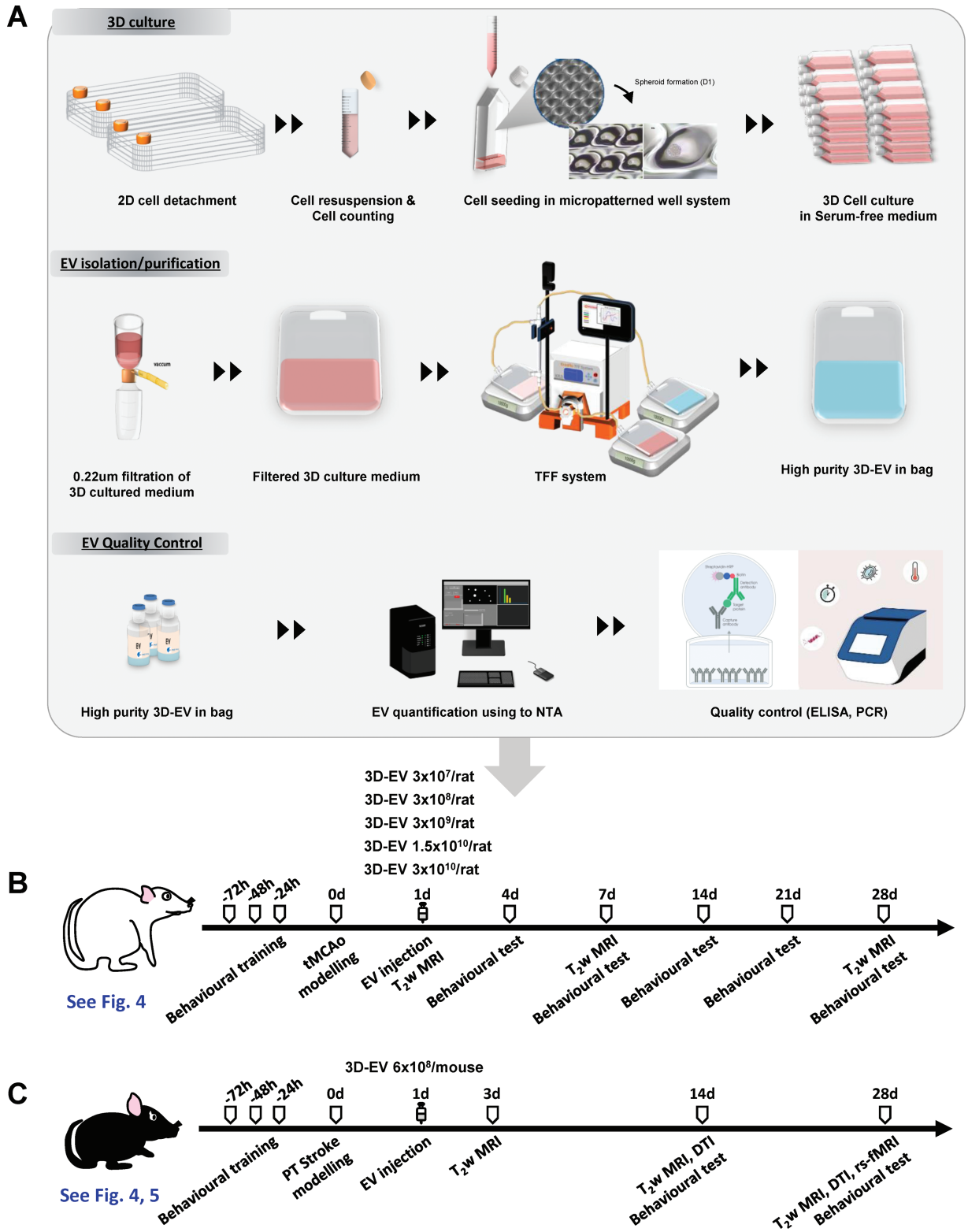

Figure 1. Scalable production process extracellular vesicles and animal study design. (**A**) Three-dimensional (3D)-mesenchymal stem cell spheroids were generated in serum-free medium using a micro-patterned well system. Extracellular vesicles (EVs) were isolated from the culture medium using a combination of filter and tangential flow filtration (TFF) system and measured for concentration and size using nanoparticle tracking (NTA); quality control was done using enzyme-linked immunosorbent assay (ELISA) and quantitative polymerase chain reaction (qPCR). (**B**) Study design: 8-week-old male Sprague-Dawley rats were trained on the ladder rung prior to transient middle cerebral artery occlusion. Infarct volume and behavioral outcomes were assessed at the indicated time points. (**C**) Study design: 8-12-week-old male C57BL/6J mice were trained on the grid prior to photothrombotic stroke. Magnetic resonance imaging for brain morphological and microstructural/functional connectivity changes and behavioral tests were assessed at the indicated time points. 2D, 2-dimensional; 3D, 3-dimensional; EVs, extracellular vesicles; NTA, nanoparticle tracking analyser.

for the processes of EV production, isolation, and quality control are shown in Fig. 1; Supplementary Fig. S1.

Characterization of EVs

Following the guidelines recommended by the International Society for Extracellular Vesicles (ISEV), known as Minimal Information for Studies of Extracellular Vesicles 2018 (MISEV2018) and the Korean FDA, the EVs isolated from the WJ-MSC cultured medium were characterized in terms of morphology, size distribution, surface markers, purity, potency marker, efficacy, stability, and safety.[12]

Nanoparticle Tracking Analysis (NTA)

The concentrations and size distributions of the isolated EVs were characterized by NTA using a NanoSight NS300 instrument (Malvern). In the NTA software program, the camera level was set to 14. NTA analysis of EVs after pre-diluted in vesicle-free PBS with EVs showed that PBS did not cause osmotic swelling of the EVs. The sample carrier cells were washed with ethanol at each EV measurement. The mean size and concentration (particles/mL) were calculated by integrating the data from 3 recordings.

Exoview Analysis

The isolated MSC-EVs were detected for CD81, CD63, and CD9 with ExoView platform (NanoView Biosciences) according to the manufacturer's instructions.

Western Blot Analysis

The EV proteins were quantified using a Pierce microBicinchoninic Acid (microBCA) Protein Assay Kit (Thermo Scientific) according to the manufacturer's instructions. See Supplementary Data for detailed methods for Western blot, transmission electron microscopy (TEM), enzyme-linked immunosorbent assay (ELISA), Exoview analysis, quantitative RT-PCR, ddPCR, small RNA sequencing, and lipidomics.

Efficacy and Dose Selection of EVs in a Rat tMCAo Model

EV Dose Selection in a Rat tMCAo Model

Various doses of EVs, ranging from 3×10^7 EVs/rat to 3×10^{10} EVs/rat, WJ-MSCs (3×10^6 cells/rat according to Zhang et al[13] or PBS were administered 1 day after onset of stroke. In total, 59 rats were randomly divided into 7 groups: the 3D-EV groups (3×10^{10} EVs/rat, $n = 7$; 1.5×10^{10} EVs/rat, $n = 6$; 3×10^9 EVs/rat, $n = 13$; 3×10^8 EVs/rat, $n = 8$; and 3×10^7 EVs/rat, $n = 7$), MSC group (3×10^6 cells/rat, $n = 3$), and PBS group ($n = 13$). In this experiment, survival rate was 84.6% in the PBS group, 100% in the MSC group, 85.7% in the 3×10^7/rat EV group, 100% in the 3×10^8/rat EV group, 92.3% in the 3×10^9/rat EV group, 100% in the 1.5×10^{10}/rat EV group, and 100% in the 3×10^{10}/rat EV group. Two animals died within 48 h after tMCAo-induced stroke and were excluded from the analysis ($n = 1$ in the PBS group and 3×10^9 EV group).

A tMCAo was induced for 90 min using an intraluminal vascular occlusion method in male Sprague-Dawley rats (8 weeks, 270-300 g), as previously described and the detailed methods are described in Supplementary Data.[5] MSC-EVs, MSCs, or PBS were slowly injected using a 1-mL syringe into the tail vein of rats 24 h after tMCAo.

Immunohistochemistry

Four weeks post-tMCAo, the effects of the 3D-EVs on neurogenesis were analyzed using a conventional immunocytochemistry protocol by immunostaining with doublecortin (DCX, an immature progenitor neuron marker) and Ki-67 (a cell proliferation marker) compared with a control (basal medium). The details of immunohistochemistry are described in the Supplementary Data.

Biodistribution Using ExoGlow-Vivo Labelled EVs

3D-EVs were labeled fluorescently with ExoGlow-Vivo EV Labeling Kit (Near IR) (Cat #EXOGV900A-1, System Biosciences) according to the individual manufacturer's instructions. The labeled EVs (3×10^{10} EVs/mouse) were administered intravenously via the tail vein in PT stroke and normal mice. Animals were imaged at various time points (3, 24, and 72 h) using IVIS In Vivo Imaging System (PerkinElmer, Waltham) and continuously observed the biodistribution for up to 72 h. Data are expressed as photons/s/cm^2/sr (sr: steradian).

Behavioral Testing

All behavioural tests including ladder walking (rat) and grid walking (mouse) were conducted by a single observer blinded to the treatment conditions up to 4 weeks after stroke induction. The details of the mouse and rat behavioral tests are described in Supplementary Data.

MRI Study in a PT Stroke Mouse Model

Experimental Design

In this study, a total of 75 mice were randomly divided into 2 treatment groups: intravenous infusion of 3D-EVs or intravenous infusion of PBS. The sample size for the MRI study was determined by a power calculation based on our previous data using rat tMCAo model with functional behavioral changes. We calculated that a sample size of 31 rats per each group was sufficient to evaluate therapeutic efficacy of EVs with an expected treatment effect of 35% (control group) or 70% (EV group), at a significance level of 5% with a power of 80%. We determined that a sample size of 40 animals per group was required considering dropout rate of 10% (mortality) and 15% (poor MRI image quality). Two animals died within 48 h after surgery (control group, $n = 2$), and 3 animals with poor MRI image quality due to motion artifact (EV group, $n = 1$; control group, $n = 2$) were excluded. Therefore, a total of 75 mice were randomly divided into 2 treatment groups: intravenous infusion of 3D-EVs (EV group, $n = 39$) or PBS (control group, $n = 36$). All EV transplantation procedures via the jugular vein were performed 1 day after the induction of the PT model. Adult male C57BL/6J mice (Orient Bio Inc.) weighing 20-25 g (8-12 weeks old) were used in this study. PT stroke was induced in the right-hand sensorimotor cortex of the mice; detailed methods are described in the Supplementary Data.

MRI Acquisition

MRI was performed using a 7T small animal MRI scanner (Bruker Biospin 70/20 USR). A quadrature birdcage coil (inner diameter = 72 mm) was used for excitation, and an actively decoupled 4-channel phased array surface coil was used to receive the signal. MRI, including T_2-weighted, DTI, and fMRI, was performed separately at 3 days, 2 weeks, and

4 weeks post-PT stroke induction according to the specific experiment, under anesthesia induced using isoflurane (5% for induction and 1.5% for maintenance, for T_2-weighted and DTI acquisition,) or a mixture of ketamine and xylazine (ketamine/xylazine 100/10 mg/kg for induction, 25/1.25 mg/kg per 45 min for maintenance, for fMRI data acquisition).[14]

MRI Analysis

All MRI data were analyzed by researchers blinded to the treatment information. The details of the MRI parameters, sequences, and processing methods are described in the Supplementary Data.

T_2-weighted images were analyzed to estimate morphological changes within the brain, such as ischaemic lesion volume and ventricular volume using ImageJ software (NIH). The infarct lesion area on each T_2-weighted image slice was identified as those voxels with a T_2 value higher than the mean + 2 SDs of normal tissue in the contralateral hemisphere.[15] Lateral and dorsal 3rd ventricular volumes were delineated with reference to the Paxinos stereotaxic mouse brain atlas.[16]

DTI image analysis was performed to observe the microstructural reorganization and structural connectivity. For the quantification of DTI-derived fractional anisotropy (FA) and fiber density (FD) values, the internal capsule (IC, peri-infarcted area), and external capsule (EC, cortico-spinal tract) were selected as regions of interest (ROI) by manually drawing on the FA map from each animal. The same ROIs were also defined on the contralateral side. Relative changes in the FA (rFA) and FD (rFD) values were calculated by dividing the values of ipsilesional ROI by those of contralesional ROI to compensate for individual variation.

Rs-fMRI data were analyzed with seed-based analysis methods. In each animal, 16 regions, including 6 cortical and 2 subcortical areas from both the ipsilesional and contralesional sides, were selected for analysis: the cingulate cortex, primary motor cortex (M1), secondary motor cortex (M2), primary somatosensory cortex forelimb (S1FL), primary somatosensory cortex hindlimb (S1HL), secondary somatosensory cortex (S2), striatum, and the thalamus. The 4 voxels that represent the center of mass at each of these regions were defined as ROIs for the seed-based analysis of the rs-fMRI data. Resting-state functional connectivity (RSFC) was extracted by calculating the cross-correlation coefficients of signal fluctuations between each ROI across all ROIs.

Statistical Analysis

All data are presented as the mean ± SD. Statistical analyses between treatment groups were performed using independent *t*-tests or one-way analysis of variance (ANOVA), Tukey's post-hoc test. To analyze the relationship between behavioral test results and MRI data, including T_2-weighted lesion/ventricle volume changes, DTI-derived rFA/rFD values, and RSFC results, Pearson correlation analysis was performed. Correlation analyses are expressed as the Pearson correlation coefficient (r) and the P value. All P-values of <0.05 were considered statistically significant. Statistical analyses were performed using the commercially available software package, SPSS version 18 (SPSS Inc.). Graphs were drawn using Graph Pad Prism 8 (Graph Pad Software Inc.).

Results

EV Characterization

The amount of EVs obtained from 3D culture system was estimated to be approximately 6417 ± 823 EVs per cell, which was much higher than the amount of EVs obtained from a conventional two-dimensional (2D) culture system (325-875 EVs per cell). The 3D-EVs had a typical round shape as seen on electron microscopy (TEM and Cryo-EM) (Fig. 2A), and the mean particle diameter was 182.5 ± 1.3 nm, and the mode particle diameter was 106.1 ± 28.5 nm (Fig. 2B). We investigated the expression of CD9, CD63, and CD81 using Exoview Tetraspanin kit. EVs were primarily captured by antibodies against each tetraspanin, and then fluorescently labeled by detection antibodies for the 3 tetraspanins. It was demonstrated that the subpopulation of CD63+ was higher than CD9+ or CD81+ (Fig. 2C). The presence of EV-specific positive markers (CD9, CD63, CD81, Hsp70, and flotillin-1) further confirmed the identity as EVs (Fig. 2D). The protein/particle ratio was 4.7 μg/10^{10} particles. Specific contaminating proteins, including histone H2A.Z, histone H3, lamin A/C, calreticulin, cytochrome C, albumin, and antibiotics, were identified by Western blot or ELISA. Histone H3, lamin A/C, calreticulin, and antibiotics were minimally detected, and histone H2A.Z, cytochrome C, and albumin were not detected (Fig. 2E).

Production Reproducibility of the 3D vs. Conventional 2D Platform

Reproducibility of 3D platform was tested in terms of the characteristics of MSC spheroid and EVs in 3 different lots. The WJ-MSCs in the microwells for each lot were well aggregated in the shape of spheroid. The size, roundness, solidity, and viability of spheroid were consistent among the different lots (Fig. 3A). The size of the 3D-spheroids was 86.74 ± 5.61 μm, and the coefficient of dispersion (CV) was 7.02%. The roundness was 0.87 ± 0.05 (CV, 5.35%), while solidity was 0.93 ± 0.02 (CV, 2.03%), indicating that WJ-MSCs were uniformly formed and well aggregated and maintained during culture for 4 days. The production reproducibility of EVs obtained from our 3D platform, as measured by the production of EV (the number and size of particle numbers and protein amount) and EV purity (particle/protein ratio), was consistent among the different lots (Fig. 3B). In addition, the expression levels of EV proteins (CD63, synthenin-1, and fibronectin), miRNAs (miR-27a-3p and miR-132-3p), and lipid composition of 3D-EV were consistent in 3 different lots (Fig. 3B).

To determine whether the production of MSC-EV is affected by donor, the characteristics of 3D-EVs and natural EVs were compared. Natural EVs showed heterogenous characteristics, in terms of the production of EV and purity depending on the donor, whereas 3D-EVs showed more homogenous characteristics compared to natural EVs (Fig. 3C).

Also, cell surface phenotypic analysis and differentiation capability test of 3D cultured MSCs showed that 3D cultivation of MSCs using a micropatterned well system did not affect the characteristics of stem cells (Supplementary Table S2 and Fig. S2). The WJ-MSC harvest yielded a homogenous population of cells with high expression of positive markers (>95% of cells) and low expression of the negative marker (<2% of cells) of MSCs. Additionally, 3D-MSCs were able to differentiate into osteoblast, adipocyte, and chondrocyte.

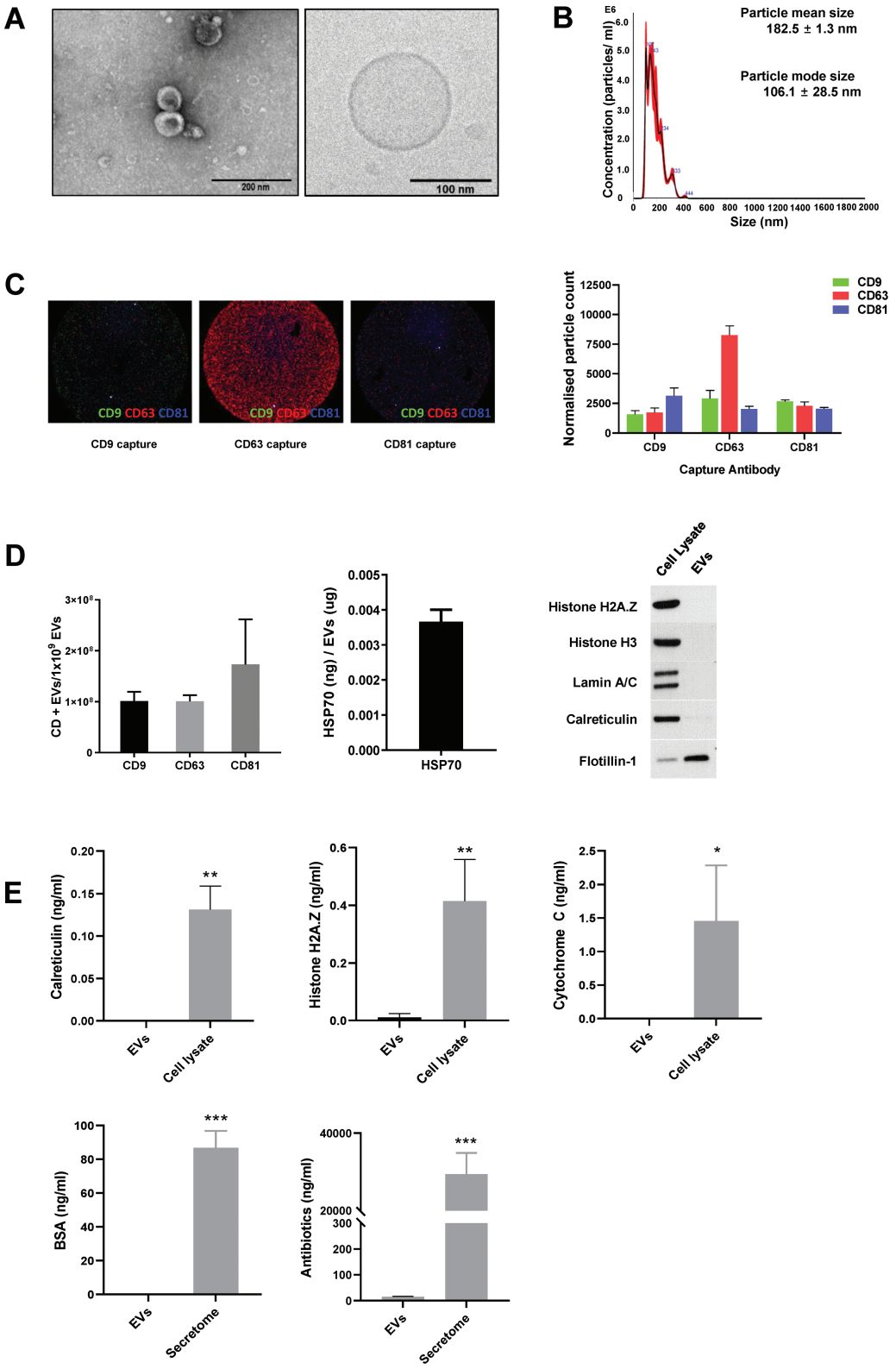

Figure 2. Characterization of extracellular vesicles (EVs) obtained from 3D culture system. (**A**) EVs imaged using electron microscopy (TEM and Cryo-EM); (**B**) histogram representing the size distributions and concentrations of the EVs using NanoSight; (**C**) The tetraspanins, including CD9, CD63, CD81 using Exoview analysis; and (**D-E**) EV positive markers, including CD9, CD63, CD81, HSP70 (enzyme-linked immunosorbent assay, ELISA), and flotillin-1 (Western blot); and EV negative markers, including calreticulin, histone H2A.Z, cytochrome C, histone H3 (Western blot), lamin A/C (Western blot), albumin, and gentamicin (ELISA).

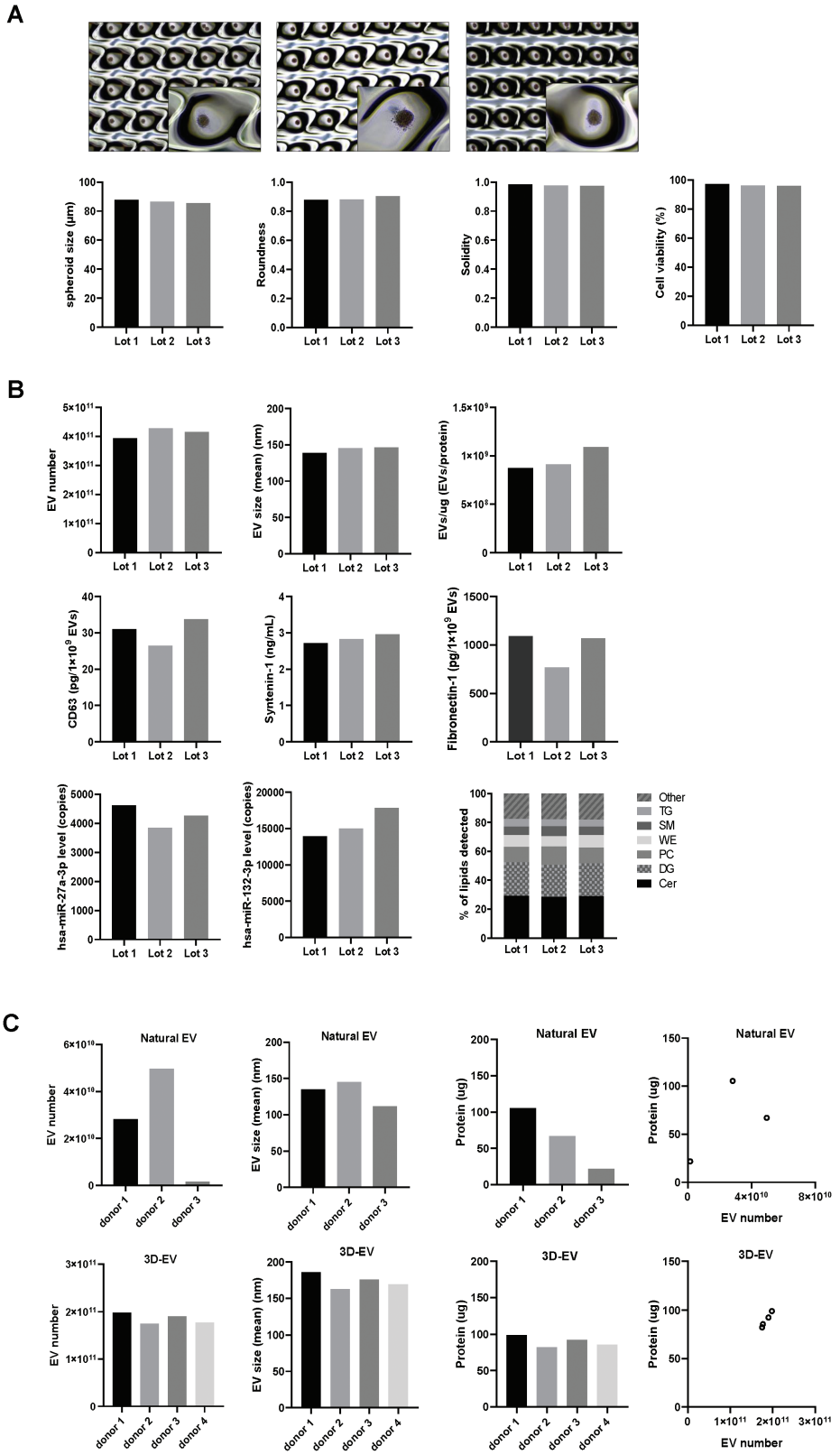

Figure 3. Production reproducibility of the 3D-EVs. Lot-to-lot variations (3 different lots from the same donor): (**A**) Four days after MSC seeding, the WJ-MSCs in the microwells for each lot were well aggregated in the shape of spheroid with a controlled size. The spheroid morphology was assessed as size, roundness, solidity, and viability. (**B**) Graph representing the number and size of EV and EV/protein ratio for each lot of 3D-EV. The expression levels of CD63, synthenin-1, and fibronectin for each lot of 3D-EV. The expression levels of miR-27a-3p and miR-132-3p for each lot of 3D-EV. The lipid composition for each lot of 3D-EV. Donor-to-donor variations: (**C**) Graph representing the number and size of EV, the amount of protein, and EV/protein ratio for each donor of EVs produced from conventional 2D-cultured MSCs (natural EV) (upper) and EVs obtained from 3D culture system (3D-EV) (lower). Cer, ceramide; DG, diglyceride; PC, phosphatidylcholine; WE, wax ester; SM, sphingomyelin; TG, triglyceride.

These results showed that 3D-MSCs maintained the representative characteristics of MSCs.

Dose De-Escalation Tests in a tMCAo Rat Model

At all tested EV doses, except the lowest dose of 3×10^7 EVs/rat, the behavioral test (ladder walking) and MRI showed enhanced functional recovery and reduced infarct volume of 3D-EV-treated rats vs. the PBS control (Fig. 4). While behavioral test showed that the effect of MSC therapy was comparable to that of the 3D-EVs, infarct volumes at 28 days were reduced in the EV groups of dose $\geq 3 \times 10^8$ EVs/rat ($P < .05$ in all cases) but not in the MSC group ($P > .05$).

To assess the in vivo effect of EVs on neuronal differentiation, immunohistochemistry was performed after the administration of PBS or EVs (3×10^9 EVs/rat, 1.5×10^{10} EVs/rat, or 3×10^{10} EVs/rat) in the rat tMCAo model. Rats that received the EVs exhibited a significant increase in the number of Ki-67/DCX double-positive cells in the subventricular zone of the ipsilateral hemispheres, at all tested EV doses (Fig. 4Ac).

For the biodistribution of EVs, ExoGlow-Vivo-labeled EVs were administered intravenously to PT stroke and normal mice, and changes were observed for 72 h using the IVIS imaging system. At 3 h after intravenous injection of EVs, more EVs were distributed in the brain in stroke mice than in normal mice, which lasted up to 72 h. On the contrary, in normal mice, the labeled EVs were rapidly excreted in the urine at 3 h of administration (Fig. 4C).

Brain Morphological Changes and Biodistribution Study in a PT Stroke Mice Model

For the mouse stroke model, the treatment dose of 3D-EVs was determined using the US FDA conversion guidance documents for industry estimating the maximum safe starting dose in adult healthy volunteers (July 2005). A minimal effective EV dose, 6×10^8 EVs/mouse (equivalent to ~3×10^9 EVs/rat), was selected for further experiments of the PT stroke mouse model.

To confirm the effects of this EV dose in PT stroke mice model, functional recovery was measured using the foot-fault test (grid-walking test). At the 28-day time point, the EV group showed a remarkable improvement in forelimb motor function, as measured using the grid walking test, compared to that in the control group ($P = .033$) (Fig. 4Bc).

To examine morphological changes of PT stroke in mice using MRI after EV therapy, the infarct lesion volume and ventricular volume were measured from T_2-weighted images (Fig. 4B; Supplementary Table S3). There was a significant difference in the ischaemic lesion volume on days 3 and 14 post-stroke between the control and EV groups ($P = .030$ and $P = .034$, respectively). Ventricular volume was measured from

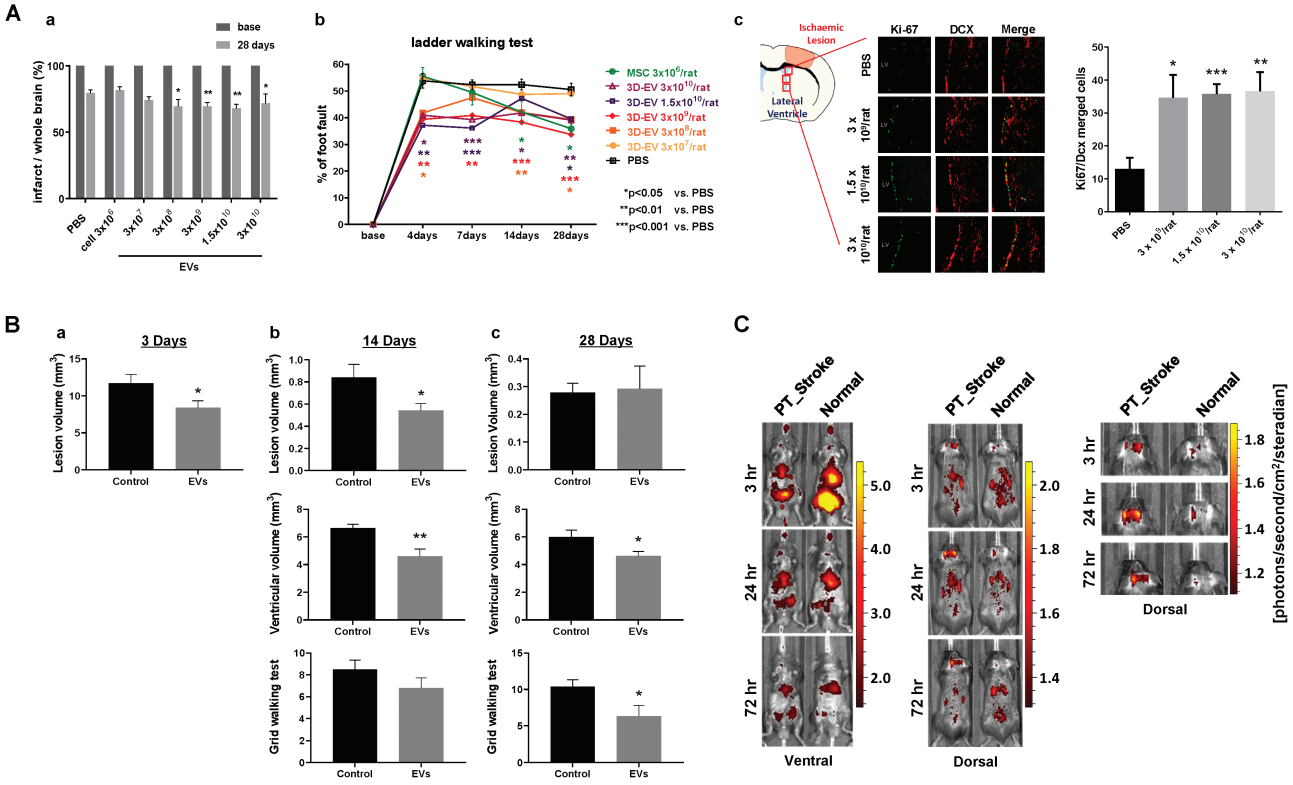

Figure 4. Selection of extracellular vesicle dose in rat stroke model (**A**) and confirmation of the minimum effective dose in a mouse stroke model (**B-C**). (**A**) Infarct volume by (a) MRI and (b) ladder walking test after treatment with MSC or different doses of extracellular vesicles obtained from 3D culture system (3D-EVs). (C) Immunohistochemistry results show significantly increased neurogenesis at all tested doses of 3D-EVs. (B) Ischemic lesion, ventricular volume, and grid walking test changes. Bar graphs representing the ischemic lesion, ventricular volume, and grid walking test at (a) 3 days (control group, $n = 20$; EV group, $n = 23$), (b) 14 days (control group, $n = 8$; EV group, $n = 10$), and (c) 28 days (control group, $n = 8$; EV group, $n = 6$) after stroke. (C) EVs isolated using TFF were labeled with the ExoGlow-Vivo dye and administered intravenously via the tail vein in stroke and normal mice. Animals were imaged at various time points (3 h, 24 h, and 72 h) using IVIS In Vivo Imaging System (PerkinElmer). Signal intensity after injection shows that EVs are rapidly taken up by target organs within 3 h of injection and decline at different rates over time. Control vs. EV group, $^*P < .05$, $^{**}P < .01$, and $^{***}P < .001$; one-way ANOVA, Tukey post-hoc test.

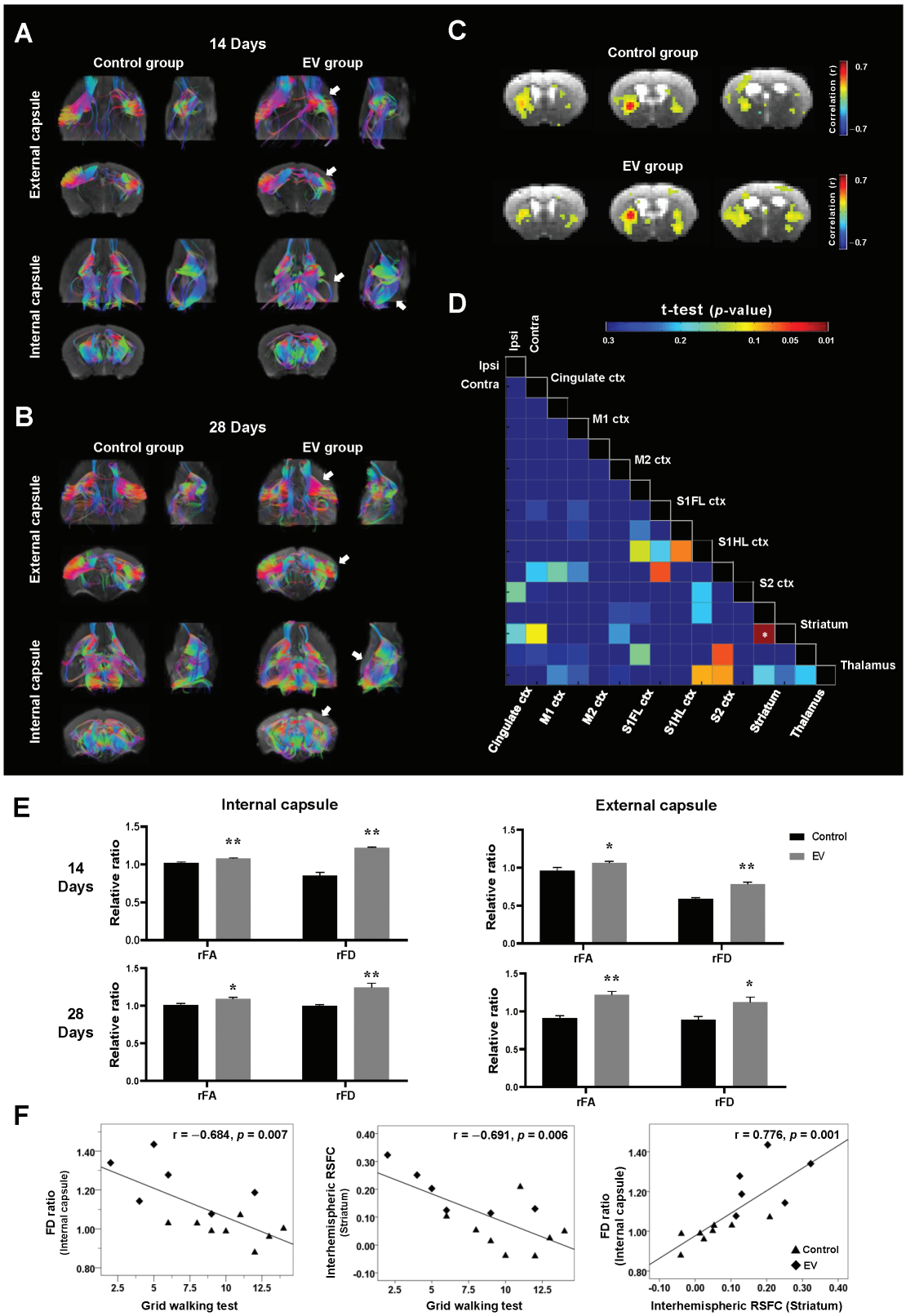

Figure 5. Correlation between behavioral recovery and MRI parameters. (**A**) DTT images from 14 days after stroke. Representative fiber tractography from the external capsule (upper) and internal capsule (below) regions of interest (ROIs) at 14 days in the control and extracellular vesicle (EV) groups. The white arrow indicates increased neural fiber tracts in the EV group. (**B**) DTT images from 28 days after stroke. Representative fiber tractography from the external capsule (upper) and internal capsule (below) ROIs at 28 days after treatment in the control and EV groups. The white arrow indicates increased neural fiber tracts in a mouse in the EV group. (**C**) Representative functional connectivity maps with seed region in the ipsilesional striatum. (**D**) Seed-based analysis of the difference in resting-state functional connectivity between the control and EV groups was performed with 16 regions of interest. Six cortical and 2 subcortical regions from both the ipsilesional and contralesional sides were selected for analysis; the cingulate cortex, primary motor cortex (M1), secondary motor cortex (M2), primary somatosensory cortex forelimb (S1FL), primary somatosensory cortex hindlimb

the lateral and dorsal third ventricles. At the 14 days time point following PT stroke, the ventricular volume of the EV group was significantly smaller than that of the control group ($P = .006$). No difference was observed in infarct volume and ventricular volume between the groups at 28 days post-stroke ($P = .875$ and $P = .052$, respectively).

Brain Microstructural/Anatomical and Functional Connectivity Changes

Brain microstructure/connectivity changes after EV treatment PT stroke mice were investigated using DTI (Fig. 5; Supplementary Table S4). The relative changes in the FA and FD values from the IC and EC ROIs were used to demonstrate the effect of treatment at 14 and 28 days after PT stroke. On 14 days post-stroke, the EV group showed a significant increase in the rFA values in both the IC and EC compared to those of the control group at 14 days ($P = .003$ and $P = .045$, respectively) and 28 days ($P = .027$, and $P < .001$, respectively).

Fig. 5A, 5B shows representative tractography images in the IC and EC ROIs at 14 and 28 days, respectively. At the 14 days time point, the reconstructed neural FD from DTT was significantly higher in the EV group than in the control group in both the IC and EC ROIs ($P < .001$, in both cases). At the 28 day time point, significant differences in the rFD values were also observed between the control and EV groups in both the IC and EC ROIs ($P < .001$ and $P = .012$, respectively).

To explore the effect of EVs on spontaneous activity changes in the brain following PT stroke, the RSFC was analyzed 28 days after PT stroke induction using seed-based analysis (Fig. 5C, 5D). From 16 ROIs, only the interhemispheric striatal functional connectivity in the EV group was significantly higher than that in the control group ($P = .008$).

The correlations between behavioral recovery tests and MRI parameters were evaluated. There was a significant correlation between functional recovery with this behavioral test and MRI parameters (Fig. 5F; Supplementary Table S5). A significant correlation was observed between the foot-fault score from the grid walking test and both the rFD of the IC ROIs ($r = –0.684$, $P = .007$) and interhemispheric RSFC of the striatum ($r = –0.691$, $P = .006$). The interhemispheric RSFC of the striatum also showed a highly significant correlation with the rFD of the IC ($r = 0.776$, $P = 0.001$).

Mechanistic Analysis of the EVs

Mechanistic analysis of the EV effects showed that compared to natural EVs, 3D-EVs were enriched with miRNAs, which mediated neurite growth of NSCs; EV and their miRNAs entered into NSCs; and EVs induced both neurogenesis (proliferation of NSCs) and neuritogenesis via miRNA-mediated actions (Fig. 6).

Small RNA sequence showed that 57 miRNAs were differentially expressed in our 3D-EVs compared with natural EVs (fold change >1.5, $P < .05$). The levels of expression of brain recovery-related miRNAs, including miR-27a-3p and miR-132-3p, were elevated in 3D-EVs than in natural EVs confirmed by qPCR ($P < .05$, in both cases). The levels of miR-27a-3p and miR-132-3p in NSCs were increased by either transfection of miR-27a-3p/miR-132-3p or treatment of miRNA-loaded EVs. The elevation of miR-27a-3p and miR-132-3p in NSCs enhanced neurogenesis, while the suppression of miR-27a-3p and miR-132-3p in NSCs reduced neurogenesis ($P < .05$, in all the cases). We identified target genes for miR-27a and miR-132 (NGAL2 and PSD95) using a target gene prediction program (Targetscan.org, v8.0). Western blotting showed that overexpression of miR-27a-3p in NSCs decreased the expression of NGAL2 protein, while overexpression of miR-132-3p in NSCs decreased the expression of PSD95 protein ($P < .05$, in both cases).

Discussion

The major findings of this study are: (1) clinical scale production of EV therapeutics is feasible using a micro-patterned well system for the 3D culture of MSCs, and compared to conventional 2D culture, the production-reproduction of EVs (the number/size of particles and EV purity) obtained from 3D platform were more consistent among different lots from the same donor and among different donors, (2) systemically administered MSC-EVs results in improvements in both functional and imaging outcomes, (3) brain microstructural and functional connectivity changes on MRI are significantly correlated with functional behavioural recovery after EV treatment, particularly relating to motor function, and (4) EV cargo, especially miRNAs, are transferred to recipient cells and mediate therapeutic effects. To our knowledge, this is the first study that used GMP-compatible methods to optimize EV production and isolation, according to the recommendations of the ISEV, for the preclinical treatment of stroke models.[12]

To date, there have been multiple studies on stem cell-derived EVs in stroke models.[3] However, the methods for EV production were not consistent: the sources of EVs, methods for their isolation, and the culturing methods and media varied greatly among studies. ISEV recommends that EV therapeutics for clinical use should have a high yield, have reproducible purity, be cultured in serum-free cell culture conditions, and consider GMP guidelines for compliance and biodistribution.[17,18] First, we used WJ-MSCs because MSCs derived from the cord/placenta showed an intermediate phenotype between adult stem cells and embryonic stem cells/induced pluripotent stem cells.[19] Second, among the various methods for EV isolation, we used the combination of filter and TFF system because it is a GMP-compliant methodology that can process large volumes.[20] Lastly, we used the 3D culture method as it allowed the large-scale production of EVs, reduced donor/batch variations, and avoided the use of serum. It is widely known that the intrinsic ability of MSCs to secrete EVs significantly declines in conventional 2D culture; thus, to reach the clinical scale production of therapeutic EVs, large batches of MSCs are decisively needed, with a significant impact on labor, time, and cost. Various methods can be used for the 3D culture of MSCs, such as suspension, hang drop, bioreactor,

(S1HL), secondary somatosensory cortex (S2), striatum, and the thalamus. (**E**) Diffusion tensor imaging (DTI) and fiber tractography results. Bar graph representing the relative fractional anisotropy (rFA) and relative fiber density (rFD) of internal capsule and external capsule at 14 days (control group, $n = 8$; EV group, $n = 10$), and 28 days (control group, $n = 8$; EV group, $n = 6$) after stroke. (**F**) Correlation between behavioral tests and MRI findings. Relationship between the grid walking test and relative fiber density (rFD) of the internal capsule, the grid walking test and interhemispheric resting-state functional connectivity (RSFC) of the striatum, and the interhemispheric RSFC of the striatum and rFD of the internal capsule. Data are presented as Pearson correlation ratios (r) and P values. Control vs. EV group, $^{\dagger}P = .052$; $^{*}P < .05$; $^{**}P < .01$; t-test.

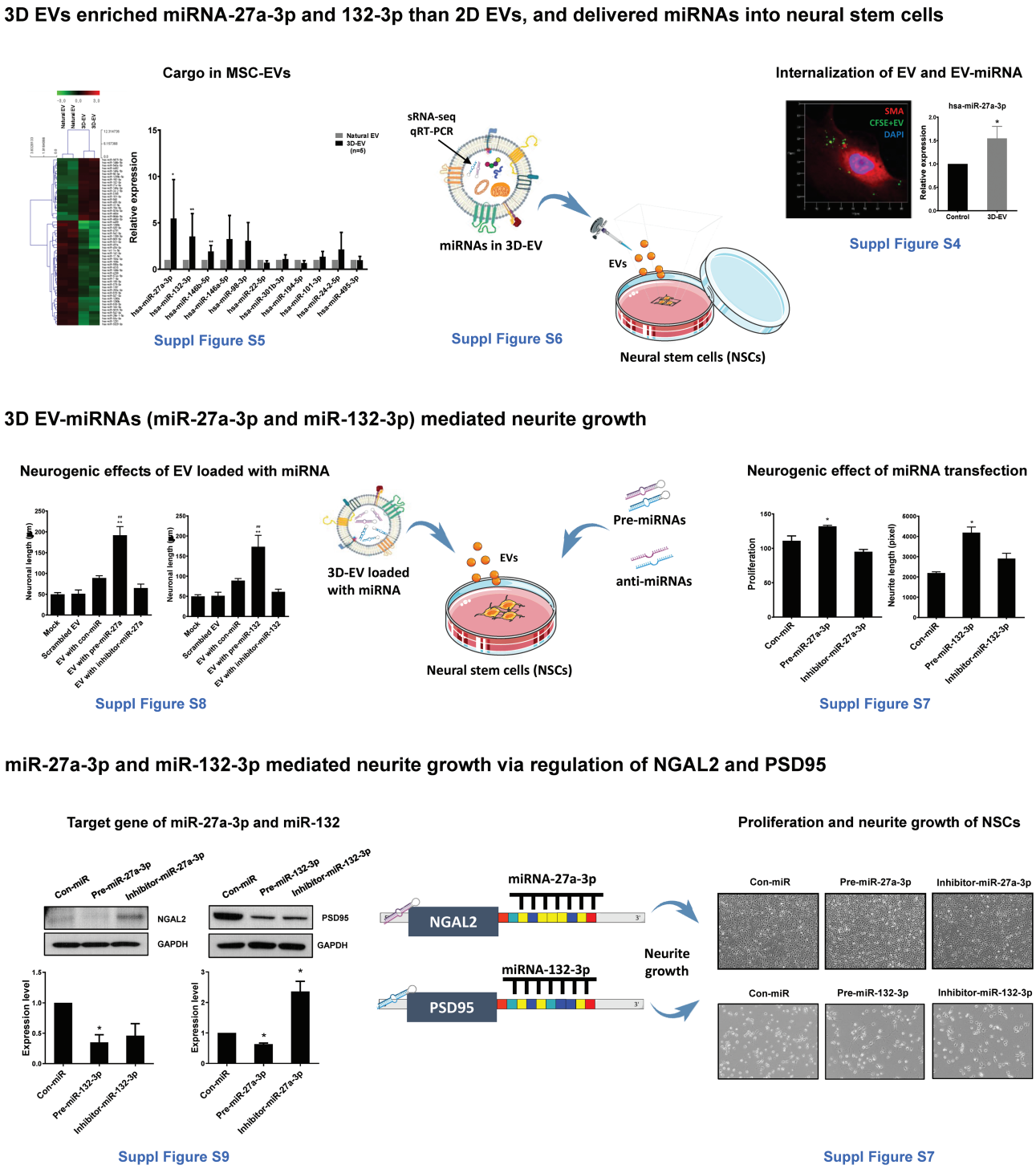

Figure 6. A schematic diagram for mechanistic analysis of the extracellular vesicles. Detailed methods and results are provided in text and Supplementary Data as indicated.

micro-patterned well, scaffold, and organoid culture, which can also be applied for EV production.[21,22] Compared to other 3D culture systems, our micro-patterned well system has advantages by generating MSC spheroids in standardized size and this method can be readily commercialized. Compared to conventional stem cell-based therapeutics, our EV therapy has potential benefits in terms of cost-effectiveness. According to the results of the previous study by Haraszti et al. and those of the present study, EVs obtained from a single mouse dose of WJ-MSCs could be applied to hundreds of mice, when WJ-MSCs were cultured in a 3D micro-patterned well system and isolated using a TFF system.[23]

Stroke is a multifaceted event and causes inflammation, apoptosis, necrosis, platelet activation, granulocyte activation, and many more biological mechanisms in the brain. Neurogenesis and neurite outgrowth are key mechanisms contributing to brain recovery after stroke, both ischaemic and hemorrhagic.[5,24] Our present study showed that MSC-EVs promoted both neuronal differentiation and the neurite outgrowth of neural stem/progenitor cells. Of the EV cargo,

miRNAs are of prime importance in mediating therapeutic effects.[1] It has been reported that EV-miRNA can regulate inflammation, apoptosis, angiogenesis, and neurogenesis.[25] In this study, we focused on neuroplasticity related to brain recovery, and our small RNA sequencing data revealed that several miRNAs were enriched in EV preparations, which were related to brain recovery. Our results showed that miR-27a-3p and miR-132-3p, mediate neurogenesis and neuritogenesis through NGAL2 and PSD95, respectively. Besides, among the miRNAs that were abundant in our EV preparations, miRNA-125b, miR-134, miR-143, and miR-24 have been shown to play an important role in neurogenesis,[26-29] and the miR-17-92 cluster, miR-21, and miR-29a contribute to the regulation of axonal growth.[30,31] Specifically, miR-134 regulates neurogenesis through Smad1/STAT3 signaling by BMP4; miR-24 mediates neural differentiation through PKCA/PLD1/SHP-1/STAT3 by HPCA[29,32-34]; miR-29 was reported to be involved in neurite elongation or remodeling via ERK signaling by 5-HT7R[31]; and the miR-17-92 cluster is involved in axonal growth through PTEN/MTOR/GSK3B activation.[35] Our EVs also contained abundant miR-146a and miR-125b, which are related to immunomodulatory activity. MiR-146a is known to be involved in T-cell differentiation by regulating transcription factors such as GATA3 and RUNX1, and miR-125b plays an important role in the immune response by inhibiting IRF-4.[36,37] Further studies are needed to investigate other roles of MSC-EVs, such as immunomodulation and neuroprotection.

Morphological changes by MRI can be sensitive indicators of neurorestoration and neuroprotection after ischaemic brain damage. Brain microstructural connectivity alterations measured by DTI and functional connectivity changes measured by rs-fMRI have been used to evaluate functional recovery in neurological diseases. The present study showed that EV therapy reduced infarct lesion volume and ventricular dilation (secondary to atrophic changes) after stroke. In particular, infarct volume was reduced in a rat tMCAo model at 28 days and in a mouse PT stroke model at 14 days. Otero-Ortega et al. observed improvements in functional recovery, fiber tract integrity, axonal sprouting, and white matter repair markers following treatment with MSC-derived EVs in a rat model of subcortical stroke.[38] In this study, infarct size was not different between the MSC-EV and control groups. The difference in the lesion volume changes between this study and our present study may be attributed to differences in the stroke model, the time of MRI scan, and EVs used. Webb et al. found that functional recovery and MRI-derived parameters are well matched after therapy with NSC-derived EVs.[39,40] DTI measures the degree of the anisotropic diffusion of water molecules in the brain using a diffusion-encoded gradient.[41-43] FA values, which are associated with neural fiber tract integrity, are used to investigate recovery after ischemic stroke.[15,38,44] With the DTI index and DTT-derived rFD values, DTI measurements indicate therapy-induced axonal remodeling after ischaemia. Rs-fMRI is an indirect measurement of resting neural activities using spontaneous fluctuations of low-frequency blood-oxygen-level-dependent signals.[45,46] The results of the present study are consistent with previous studies showing that interhemispheric RSFCs are reduced in the acute phase following ischaemic stroke, while increased functional connectivity in motor-related brain regions is associated with spontaneous or therapy-induced recovery in the late phase.[47-50] In the present study, we observed that the increased rFA and rFD values in the IC and the interhemispheric RSFC values of the striatum were both associated with functional behavioral improvement after MSC-EV therapy. The IC contains corticospinal tracts that connect the spinal cord to the primary motor cortex, whereas the striatum plays a critical role in sensorimotor function. From our correlation analyses between the grid walking test and the rFD of the IC or the interhemispheric RSFC of the striatum, MRI indices were significantly correlated with the treatment-induced recovery of motor function. Additionally, the functional connectivity measured by rs-fMRI and microstructural connectivity from DTI were significantly correlated with each other. These results suggest that brain microstructural/functional connectivity changes from MRI may be a potential indicator of functional recovery following MSC-EV treatment and that such connectivity changes are one of the MSC-EV mechanisms involved in recovery after stroke.

The strengths of this study include: (1) the effect of MSC-EV treatment was tested in different species (mouse and rat) and in different stroke models (transient MCAo [suture model] and permanent [photothrombotic model]), which showed a consistent finding of therapeutic benefit; (2) objective measurements of neuroplasticity were performed using MRI to investigate mechanisms underlying MSC-EV induced recovery after stroke[4]. However, several limitations deserve to be mentioned. First, although our present and previous biodistribution studies showed that MSC-EVs were quickly distributed and delivered to the infarcted hemisphere, quantitative analyses measuring serial changes at different time points are needed. Currently, with radioisotope labeled EVs, measurements with single photon emission computed tomography imaging and gamma counter are ongoing for quantitative evaluation of biodistribution. Second, although we performed multiple analyses including small RNA sequencing, mechanisms studies, and target gene analysis, further studies on the proteomics, lipidomics, and glycomics of EVs are needed for the multinomic characterization of EVs. Third, only one behavioral test was used from each rat and mice experimental stroke model, although we also evaluated specific MRI measurements for brain morphological/functional recovery. Fourth, the therapeutic efficacy of MSC-EVs over time in this study was investigated using separate cohorts of animals; therefore, the measured MRI parameters were different. In addition to investigating the effects of EV therapy as a function of age, comorbidity, and sex, future studies should undertake the longitudinal measurement of outcomes in the same animal to develop potential imaging biomarkers to assess EV therapy. The use of task-induced fMRI may also provide more prominent information regarding functional recovery in the area damaged by ischemia, compared to that by examining only resting-state functional connectivity.

In conclusion, the present study indicates that our scalable 3D-bioprocessing production method for clinical-scale MSC-EV therapy is feasible, reduces donor/batch variations, and improves functional recovery following experimental stroke. EVs obtained from 3D platform enriched microRNAs with molecular functions associated with neurogenesis, and EV incorporated miR-27a-3p and miR-132-3p mediate these therapeutic effects. In addition, morphological and brain microstructural/functional connectivity changes on multimodal MRI likely contribute to the EV therapeutic enhancement of recovery after stroke, and may provide imaging biomarkers for functional recovery following EV therapy.

Acknowledgments

We would like to thank the Animal Research and Molecular Imaging Center at Samsung Medical Center for their help in acquiring animal MRI.

Funding

S&E Bio, Inc. provided support for this study in the form of salaries for EHK, EKS, and JHS. The specific roles of these authors are articulated in the "author contributions" section. This study was supported in part by a grant from the Technology Innovation Program (1415174804) funded By the Ministry of Trade, Industry & Energy (MOTIE, Korea). The funders had no role in study design, data collection and analysis, decision to publish, or preparation of the manuscript.

Conflict of Interest

The authors of this manuscript have the following competing interests: EHK, EKS, and JHS are paid employees of S&E Bio, Inc. S&E bio, Inc have filed patent application related to the methods described in this study, but there is no marketing product to declare. This does not affect our adherence to the data and material-sharing policies of the STEM CELLS Translational Medicine policies on sharing data and materials.

Author Contributions

J.P.S., E.H.K.: conception and design, collection and/or assembly of data, data analysis and interpretation, manuscript writing. E.K.S., D.H.K., J.H.S., M.J.O.: provision of study material or patients, collection and/or assembly of data. J.M.C.: revision of study for important intellectual content. M.C.: revision the report and giving scientific advice. O.Y.B.: conception and design, financial support, collection and/or assembly of data, data analysis and interpretation, manuscript writing, final approval of manuscript.

Data Availability

The data underlying this article will be shared on reasonable request to the corresponding author.

Supplementary Material

Supplementary material is available at *Stem Cells Translational Medicine* online.

References

1. Zhang ZG, Buller B, Chopp M. Exosomes—beyond stem cells for restorative therapy in stroke and neurological injury. *Nat Rev Neurol*. 2019;15(4):193-203. https://doi.org/10.1038/s41582-018-0126-4
2. Xin H, Li Y, Cui Y, et al. Systemic administration of exosomes released from mesenchymal stromal cells promote functional recovery and neurovascular plasticity after stroke in rats. *J Cereb Blood Flow Metab*. 2013;33(11):1711-1715.
3. Bang OY, Kim EH. Mesenchymal stem cell-derived extracellular vesicle therapy for stroke: challenges and progress. *Front Neurol*. 2019;10:211. https://doi.org/10.3389/fneur.2019.00211
4. Chen J, Chopp M. Exosome therapy for stroke. *Stroke*. 2018;49(5):1083-1090. https://doi.org/10.1161/STROKEAHA.117.018292
5. Moon GJ, Sung JH, Kim DH, et al. Application of mesenchymal stem cell-derived extracellular vesicles for stroke: biodistribution and MicroRNA study. *Transl Stroke Res*. 2019;10(5):509-521. https://doi.org/10.1007/s12975-018-0668-1
6. Bang OY, Kim EH, Cho YH, et al. Circulating extracellular vesicles in stroke patients treated with mesenchymal stem cells: a biomarker analysis of a randomized trial. *Stroke*. 2022;53(7):STROKEAHA121036545.
7. Bari E, Perteghella S, Di Silvestre D, et al. Pilot production of mesenchymal stem/stromal freeze-dried secretome for cell-free regenerative nanomedicine: a validated GMP-compliant process. *Cells*. 2018;7(11):190190. https://doi.org/10.3390/cells7110190
8. Bari E, Perteghella S, Catenacci L, et al. Freeze-dried and GMP-compliant pharmaceuticals containing exosomes for acellular mesenchymal stromal cell immunomodulant therapy. *Nanomedicine*. 2019;14(6):753-765. https://doi.org/10.2217/nnm-2018-0240
9. Pachler K, Lener T, Streif D, et al. A good manufacturing practice-grade standard protocol for exclusively human mesenchymal stromal cell-derived extracellular vesicles. *Cytotherapy*. 2017;19(4):458-472. https://doi.org/10.1016/j.jcyt.2017.01.001
10. Cha JM, Shin EK, Sung JH, et al. Efficient scalable production of therapeutic microvesicles derived from human mesenchymal stem cells. *Sci Rep*. 2018;8(1):1171. https://doi.org/10.1038/s41598-018-19211-6
11. Kilkenny C, Browne WJ, Cuthill IC, Emerson M, Altman DG. Improving bioscience research reporting: the ARRIVE guidelines for reporting animal research. *PLoS Biol*. 2010;8(6):e1000412. https://doi.org/10.1371/journal.pbio.1000412
12. Thery C, Witwer KW, Aikawa E, et al. Minimal information for studies of extracellular vesicles 2018 (MISEV2018): a position statement of the International Society for Extracellular Vesicles and update of the MISEV2014 guidelines. *J Extracell Vesicles*. 2018;7(1):1535750. https://doi.org/10.1080/20013078.2018.1535750
13. Zhang L, Li Y, Zhang C, et al. Delayed administration of human umbilical tissue-derived cells improved neurological functional recovery in a rodent model of focal ischemia. *Stroke*. 2011;42(5):1437-1444. https://doi.org/10.1161/STROKEAHA.110.593129
14. Jung WB, Shim H-J, Kim S-G. Mouse BOLD fMRI at ultrahigh field detects somatosensory networks including thalamic nuclei. *Neuroimage*. 2019;195:203-214. https://doi.org/10.1016/j.neuroimage.2019.03.063
15. Jiang Q, Thiffault C, Kramer BC, et al. MRI detects brain reorganization after human umbilical tissue-derived cells (hUTC) treatment of stroke in rat. *PLoS One*. 2012;7(8):e42845. https://doi.org/10.1371/journal.pone.0042845
16. Franklin KB, Paxinos G. *The Mouse Brain in Stereotaxic Coordinates*. Vol 3: Academic press, 2008.
17. Reiner AT, Witwer KW, van Balkom BWM, et al. Concise review: developing best-practice models for the therapeutic use of extracellular vesicles. *Stem Cells Transl Med*. 2017;6(8):1730-1739. https://doi.org/10.1002/sctm.17-0055
18. Witwer KW, Van Balkom BWM, Bruno S, et al. Defining mesenchymal stromal cell (MSC)-derived small extracellular vesicles for therapeutic applications. *J Extracell Vesicles*. 2019;8(1):1609206. https://doi.org/10.1080/20013078.2019.1609206
19. Loukogeorgakis SP, De Coppi P. Concise review: amniotic fluid stem cells: the known, the unknown, and potential regenerative medicine applications. *Stem Cells*. 2017;35(7):1663-1673. https://doi.org/10.1002/stem.2553
20. Watson DC, Yung BC, Bergamaschi C, et al. Scalable, cGMP-compatible purification of extracellular vesicles carrying bioactive human heterodimeric IL-15/lactadherin complexes. *J Extracell Vesicles*. 2018;7(1):1442088. https://doi.org/10.1080/20013078.2018.1442088

21. Lv D, Hu Z, Lu L, Lu H, Xu X. Three-dimensional cell culture: a powerful tool in tumor research and drug discovery. *Oncol Lett*. 2017;14(6):6999-7010. https://doi.org/10.3892/ol.2017.7134
22. Zhang Y, Chopp M, Zhang ZG, et al. Systemic administration of cell-free exosomes generated by human bone marrow derived mesenchymal stem cells cultured under 2D and 3D conditions improves functional recovery in rats after traumatic brain injury. *Neurochem Int*. 2017;111:69-81. https://doi.org/10.1016/j.neuint.2016.08.003
23. Haraszti RA, Miller R, Stoppato M, et al. Exosomes produced from 3D cultures of MSCs by tangential flow filtration show higher yield and improved activity. *Mol Ther*. 2018;26(12):2838-2847. https://doi.org/10.1016/j.ymthe.2018.09.015
24. Otero-Ortega L, Gómez de Frutos MC, Laso-García F, et al. Exosomes promote restoration after an experimental animal model of intracerebral hemorrhage. *J Cereb Blood Flow Metab*. 2018;38(5):767-779.
25. Shojaati G, Khandaker I, Funderburgh ML, et al. Mesenchymal stem cells reduce corneal fibrosis and inflammation via extracellular vesicle-mediated delivery of miRNA. *Stem Cells Transl Med*. 2019;8(11):1192-1201. https://doi.org/10.1002/sctm.18-0297
26. Lattanzi A, Gentner B, Corno D, et al. Dynamic activity of miR-125b and miR-93 during murine neural stem cell differentiation in vitro and in the subventricular zone neurogenic niche. *PLoS One*. 2013;8(6):e67411. https://doi.org/10.1371/journal.pone.0067411
27. Xiao Y, Geng F, Wang G, et al. Bone marrow-derived mesenchymal stem cells-derived exosomes prevent oligodendrocyte apoptosis through exosomal miR-134 by targeting caspase-8. *J Cell Biochem*. 2019;120(2):2109-2118. https://doi.org/10.1002/jcb.27519
28. Quaranta MT, Spinello I, Paolillo R, et al. Identification of β-dystrobrevin as a direct target of miR-143: involvement in early stages of neural differentiation. *PLoS One*. 2016;11(5):e0156325. https://doi.org/10.1371/journal.pone.0156325
29. Kang M-J, Park S-Y, Han J-S. MicroRNA-24-3p regulates neuronal differentiation by controlling hippocalcin expression. *Cell Mol Life Sci*. 2019;76(22):4569-4580. https://doi.org/10.1007/s00018-019-03290-3
30. Jamsuwan S, Klimaschewski L, Hausott B. Simultaneous knockdown of Sprouty2 and PTEN promotes axon elongation of adult sensory neurons. *Front Cell Neurosci*. 2019;13:583. https://doi.org/10.3389/fncel.2019.00583
31. Volpicelli F, Speranza L, Pulcrano S, et al. The microRNA-29a modulates serotonin 5-HT7 receptor expression and its effects on hippocampal neuronal morphology. *Mol Neurobiol*. 2019;56(12):8617-8627. https://doi.org/10.1007/s12035-019-01690-x
32. Park S-Y, Yoon SN, Kang M-J, et al. Hippocalcin promotes neuronal differentiation and inhibits astrocytic differentiation in neural stem cells. *Stem Cell Rep*. 2017;8(1):95-111. https://doi.org/10.1016/j.stemcr.2016.11.009
33. Gaughwin P, Ciesla M, Yang H, Lim B, Brundin P. Stage-specific modulation of cortical neuronal development by Mmu-miR-134. *Cereb Cortex*. 2011;21(8):1857-1869. . https://doi.org/10.1093/cercor/bhq262
34. Cole AE, Murray SS, Xiao J. Bone morphogenetic protein 4 signalling in neural stem and progenitor cells during development and after injury. *Stem Cells Int*. 2016;2016:1-16. . https://doi.org/10.1155/2016/9260592
35. Zhang Y, Ueno Y, Liu XS, et al. The microRNA-17–92 cluster enhances axonal outgrowth in embryonic cortical neurons. *J Neurosci*. 2013;33(16):6885-6894. . https://doi.org/10.1523/jneurosci.5180-12.2013
36. Saki N, Abroun S, Soleimani M, et al. The roles of miR-146a in the differentiation of Jurkat T-lymphoblasts. *Hematology*. 2014;19(3):141-147. . https://doi.org/10.1179/1607845413Y.0000000105
37. Chaudhuri AA, So AY-L, Sinha N, et al. MicroRNA-125b potentiates macrophage activation. *J Immunol*. 2011;187(10):5062-5068. . https://doi.org/10.4049/jimmunol.1102001
38. Otero-Ortega L, Laso-García F, del Carmen Gómez-de Frutos M, et al. White matter repair after extracellular vesicles administration in an experimental animal model of subcortical stroke. *Sci Rep*. 2017;7(1):44433.
39. Webb RL, Kaiser EE, Jurgielewicz BJ, et al. Human neural stem cell extracellular vesicles improve recovery in a porcine model of ischemic stroke. *Stroke J Cereb Circ*. 2018;49(5):1248-1256.
40. Webb RL, Kaiser EE, Scoville SL, et al. Human neural stem cell extracellular vesicles improve tissue and functional recovery in the murine thromboembolic stroke model. *Transl Stroke Res*. 2018;9(5):530-539. . https://doi.org/10.1007/s12975-017-0599-2
41. Basser PJ, Jones DK. Diffusion-tensor MRI: theory, experimental design and data analysis—a technical review. *NMR Biomed*. 2002;15(7-8):456-467. . https://doi.org/10.1002/nbm.783
42. Beaulieu C. The basis of anisotropic water diffusion in the nervous system—a technical review. *NMR Biomed*. 2002;15(7-8):435-455. . https://doi.org/10.1002/nbm.782
43. Tournier JD, Mori S, Leemans A. Diffusion tensor imaging and beyond. *Magn Reson Med*. 2011;65(6):1532-1556. https://doi.org/10.1002/mrm.22924
44. van Velthoven CT, van de Looij Y, Kavelaars A, et al. Mesenchymal stem cells restore cortical rewiring after neonatal ischemia in mice. *Ann Neurol*. 2012;71(6):785-796. https://doi.org/10.1002/ana.23543
45. Biswal B, Zerrin Yetkin F, Haughton VM, Hyde JS. Functional connectivity in the motor cortex of resting human brain using echo-planar MRI. *Magn Reson Med*. 1995;34(4):537-541. https://doi.org/10.1002/mrm.1910340409
46. Raichle ME. The restless brain: how intrinsic activity organizes brain function. *Philos Trans R Soc B Biol Sci*. 2015;370(1668):20140172. . https://doi.org/10.1098/rstb.2014.0172
47. Park C-h, Chang WH, Ohn SH, et al. Longitudinal changes of resting-state functional connectivity during motor recovery after stroke. *Stroke J Cereb Circ*. 2011;42(5):1357-1362.
48. Thiel A, Vahdat S. Structural and resting-state brain connectivity of motor networks after stroke. *Stroke J Cereb Circ*. 2015;46(1):296-301.
49. Liang S, Lin Y, Lin B, et al. Resting-state functional magnetic resonance imaging analysis of brain functional activity in rats with ischemic stroke treated by electro-acupuncture. *J Stroke Cerebrovasc Dis*. 2017;26(9):1953-1959. https://doi.org/10.1016/j.jstrokecerebrovasdis.2017.06.018
50. Cha J, Kim ST, Jung WB, et al. Altered white matter integrity and functional connectivity of hyperacute-stage cerebral ischemia in a rat model. *Magn Reson Imaging*. 2016;34(8):1189-1198. https://doi.org/10.1016/j.mri.2016.04.004